J Mater Sci: Mater Med (2008) 19:3295–3302
DOI 10.1007/s10856-008-3466-6

Biomimetic formation of hydroxyapatite investigated by analytical techniques with high resolution

R. B. Heimann · T. P. Ntsoane · C. A. Pineda-Vargas · W. J. Przybylowicz · M. Topić

Received: 31 January 2008 / Accepted: 25 April 2008 / Published online: 16 May 2008
© Springer Science+Business Media, LLC 2008

Abstract Morphology, phase and chemical compositions of atmospheric plasma-sprayed (APS) hydroxyapatite (HAp) coatings were investigated by scanning electron microscopy (SEM), X-ray powder diffraction (XRD), proton-induced X-ray emission (PIXE) and Rutherford backscattering spectrometry (RBS). The study involved as-sprayed coatings and coatings incubated in simulated body fluid (rSBF) for up to 56 days. The results obtained using combined contributions from three complementary analytical techniques confirm that secondary Ca-deficient defect hydroxyapatite precipitated by a biomimetic process from the simulated body fluid onto the HAp coating surface after a prolonged induction time. Owing to its sensitivity proton-induced X-ray emission (PIXE) provides information on in vitro resorption of calcium phosphate ceramics and dynamic dissolution/precipitation events occurring during the incubation process.

W. J. Przybylowicz: On leave from the Faculty of Physics and Applied Informatics, AGH University of Science and Technology, Krakow, Poland.

R. B. Heimann (✉)
University Center of Medical Technology (UZMT), Ruhr-Universität Bochum, Bochum, Germany
e-mail: robert.heimann@ocean-gate.de

T. P. Ntsoane · C. A. Pineda-Vargas · W. J. Przybylowicz · M. Topić
Materials Research Group, iThemba Labs, Somerset West, South Africa

T. P. Ntsoane
Department of Physics, University of Cape Town, Cape Town, South Africa

C. A. Pineda-Vargas
Groote Schuur Hospital, Observatory, South Africa

1 Introduction

Thermal spraying of hydroxyapatite ($Ca_{10}(PO_4)_6(OH)_2$, HAp) is widely used to produce various coatings in orthopedics and dentistry [1], applied in particular to the stems of hip endoprostheses to enhance their biological fixation as HAp is osseoconductive and hence capable of rapidly forming a chemical bond with living bone tissue. The techniques generally involve introducing powder particles into a plasma jet, which are being melted and accelerated towards a metal substrate under either low pressure (LPPS) or atmospheric plasma spraying (APS) conditions [2]. However, since there exist several unresolved issues pertaining to quality and reliability of these bioconductive coatings many studies were conducted during the last several decades centred around applying alternate spraying techniques, and improving microstructural and mechanical properties such as coating porosity, adhesion to the metallic implant body and other essential properties [3–10].

To improve the reliability of these coatings for human implants application it is vital to understand the changes that morphology, and chemical and phase compositions of the hydroxyapatite coatings undergo when brought in contact with living tissue. In this study, hydroxyapatite (HAp) coatings were deposited onto Ti6Al4V substrates by APS followed by incubation in revised simulated body fluid (rSBF) [11] to assess their possible biofunctional performance. The compositional changes of the coatings caused by the incubation process were investigated after 1, 7, 28 and 56 days. It is believed that dynamic reactions at the HAp coating/bone interface result from a sequence of events involving, among others, complex processes including the formation of carbonate hydroxyapatite by a dissolution–precipitation process [12].

1.1 Complementarities of analytical techniques

Both conventional and novel analytical techniques have been applied to understand the physico-chemical processes that take place during every single step from HAp coating deposition to in vitro incubation process in simulated body fluid to essential physiological processes governing the in vivo performance. The aim of this study is directed towards the characterisation of bioconductive hydroxyapatite coatings using different complementary techniques: X-ray powder diffraction (XRD), scanning electron microscopy (SEM), proton-induced X-ray emission (PIXE) and Rutherford backscattering spectroscopy (RBS). While the two former techniques are being routinely used to determine coating phase composition and microstructure, the application of PIXE and RBS is relatively new to the field of biomedical engineering. PIXE can detect elements, and map minor and trace elements in the coatings and tissue surrounding the implants at concentration levels as low as 500 $\mu g\ g^{-1}$ and below [13]. In this study, the changes in concentration and the 2-D distribution of Ca, P and trace elements were recorded using PIXE technique. Furthermore, since PIXE is a non-destructive technique it is a very useful tool for monitoring the changes in concentration of elements contained in bioceramics since their concentrations are in constant evolution with time after implantation [12, 34]. PIXE with its good sensitivity for transition elements with medium atomic mass provides a novel approach towards studying bioconductive coatings and their in vivo alteration products. Rutherford backscattering spectroscopy uses backscattered alpha particles within the surface of the material to obtain quantitative information on the major/minor components that cannot be detected with PIXE. Compared to PIXE and conventional XRD that provide analytical information down to several micrometers into the bulk coating, RBS probes only the immediate surface area.

2 Materials and methods

The materials used in this study were commercially available medical-grade HAp powder (Plasma Biotal Ltd., Tideswell, North Derbyshire, UK) and a mill-annealed Ti6Al4V alloy (6.12 at% Al, 4.20 at% V, 0.17 at% Fe, 0.01 at% C, 0.105 at% O, 0.005 at% N, 0.003 at% H, Ti bal.) as substrate material. The HAp powder (CAPTAL 90; particle size range 120 ± 20 μm) consisted of 97.6 ± 0.8 mass% hydroxyapatite, HAp, 0.30 ± 0.55 mass% tricalcium phosphate, TCP and 2.1 ± 0.8 mass% tetracalcium phosphate, TTCP.

The powder was atmospherically plasma sprayed onto machined "dog bone" samples (130 × 22.5 × 2 mm) and "square coupons" (20 × 20 × 2 mm) to a thickness of about 200 μm using a PT M1000 (Plasmatechnik Wohlen, Switzerland) APS-system equipped with a Sulzer Metco F4 MB plasmatron using the spraying parameters listed in Table 1 [14]. To improve bonding between HAp and the metal substrate, prior to coating the samples of either type were grit-blasted for 90 s with corundum (grain size between 0.5 and 1.0 mm) using an air pressure of 4 bars at an angle of 90° to produce a surface roughness of 2.0 μm. Subsequently the specimens were ultrasonically cleaned in a solution of 10% Tickopur^{TM} in deionised water at 40°C for 10 min. The Ti6Al4V substrates were preheated to 400°C prior to spray coating. A spray pattern was produced by six partially overlapping horizontal passes of the plasma jet, each one followed by an intercycle cooling period before the next cycle started. To avoid undue heating during spraying the substrates were cooled from the back with an argon stream.

After coating the samples were rinsed with methanol to remove residual loose powder particles and dried in a dust-free air environment. Subsequently eight coupons and eight "dog-bone" samples were incubated between 1 and 56 days in rSBF (Table 2) under physiological conditions (at 37 ± 0.5°C) to simulate the effect of the biological environment. After incubation, the samples were rinsed with deionised water and dried at 100°C for 24 h. To stabilise the rSBF, i.e. to prevent precipitation of calcium carbonate 15 ml of a buffer solution (11.93 g/l HEPES + 40 g/l NaOH) were added per litre of rSBF.

Small blocks (typically 10 × 10 mm) of HAp coatings peeled off from "dog bone" tensile samples were used for

Table 1 Plasma spray parameters [14]

Parameter	Unit	Value
Primary plasma gas (argon)	slpm	45
Secondary plasma gas (hydrogen)	slpm	6.5
Powder carrier gas (argon)	slpm	5.0
Relative powder feed rate	%	20
Relative hopper stirrer rate	%	40
Spray distance	mm	90
Plasma power	kW	30–32
Traverse speed	m/s	6
Number of traverses		6

Table 2 Composition of rSBF in mmol/l [11]

Na^+	Ca^{2+}	K^+	Cl^-	Mg^{2+}	HPO_4^{2-}	SO_4^{2-}	HCO_3^-
142.0	2.5	5.0	103.0	1.5	1.0	0.5	27.0

HEPES: [2-(4-(2-hydroxyethyl)-1-piperazinyl) ethan] sulfonic acid + 1 M NaOH

coating characterisation by scanning electron microscopy, micro-PIXE mapping and Rutherford Backscattering Spectrometry (RBS), while the coated square coupons were used for phase analysis by conventional X-ray diffraction.

Scanning electron microscopy (Cambridge Stereoscan 200×) was used to investigate the effects of incubation time on HAp coating morphology. The study included both the coupons and HAp blocks (top-side coating), which were carbon coated to prevent charging.

Crystalline phase contents of the coatings deposited onto the square coupons were determined by X-ray diffraction (URD 6, Freiberger Präzisionsmechanik). Measurements were performed using CoK_{α} radiation generated by an X-ray tube operated at 40 kV and 35 mA with 2θ angle ranging from 25° to 55° and at a scan step size of 0.03°. For quantitative data, Rietveld refinement was carried out using structural models of different calcium phosphate phases obtained from the ICSD (Inorganic Crystal Structure Database).

Pieces of hydroxyapatite coating (top of coatings facing the solution) were irradiated using the Nuclear Microprobe (NMP) facility at iThemba LABS [15–17]. Proton beams with energies of 1.5 MeV were selected for bombardment of particular micro-regions of the HAp coatings. Beam currents of 200–400 pA were used to ensure that no evaporation of constituents occurred due to a possible rise in temperature generated in the sample volume. Microregions were scanned with a proton probe beam of 2 and 4 μm diameter. A scan size of 128 × 128 pixels was used to ensure sufficient resolution for mapping visualisation. Areas of approximately 250 × 250 μm^2 were selected on the HAp coatings for analysis. True overlap-resolved elemental maps as well as total micro-PIXE data were obtained using the Dynamic Analysis (DA) method. Off-line analyses of experimental data recorded as event-by-event computer files were obtained with the software package Geo-PIXE II [18].

To quantify the Ca/P stoichiometric ratio in the hydroxyapatite layers, RBS with 2.0 MeV alpha particle beam was used. The software package RUMP [19] was used for the evaluation of the backscattered spectra.

3 Results and discussion

3.1 Scanning electron microscopy

SEM micrographs show that the HAp coating surface morphology changed dramatically after prolonged incubation time in rSBF (Fig. 1a, b). It was found that coating morphology remained almost unaffected throughout a short incubation time of a few days while after 7 days of incubation precipitation was noted of secondary calcium phosphate from the simulated body fluid [5]. Since rSBF is supersaturated with respect to both hydroxyapatite and octacalcium phosphate (OCP) at the experimental pH of 7.4 these phases are thermodynamically favoured and should precipitate spontaneously. However, it has frequently been observed [20–22] that metastable precursor phases with high solubilities appear first according to Ostwald's principle since the energies required to nucleate these metastable products are much lower than those of the thermodynamically stable target phases. For example, the nucleation rate of OCP is higher by 10 orders of magnitude than that of HAp under physiological conditions (pH = 7.4). In addition HAp has a lower rate of growth compared to OCP when normalized for surface area [23, 24]. Kinetically, therefore, OCP may form exclusively on surfaces in the presence of suitable growth sites. These growth sites, however, may be blocked by adsorption of ions such as Mg and Sr. Indeed, Mg ions were found to hinder kinetically the nucleation and subsequent growth of OCP and HAp by competing for lattice sites with the chemically similar but larger calcium ions [25, 26]. On the other hand, incorporation of Sr into the structure of hydroxyapatite appears to increases the solubility [27].

Also, complex organic molecules were found to absorb easily at HAp and other calcium phosphate surfaces blocking selectively preferential growth sites either completely [28, 29] or else lend support to the hypothesis that hierarchical structures in nature result from cooperative interaction between organic assembly and crystal growth [30]. Experimental evidence exists [31] obtained by in situ synchrotron small-angle X-ray scattering (SAXS) that

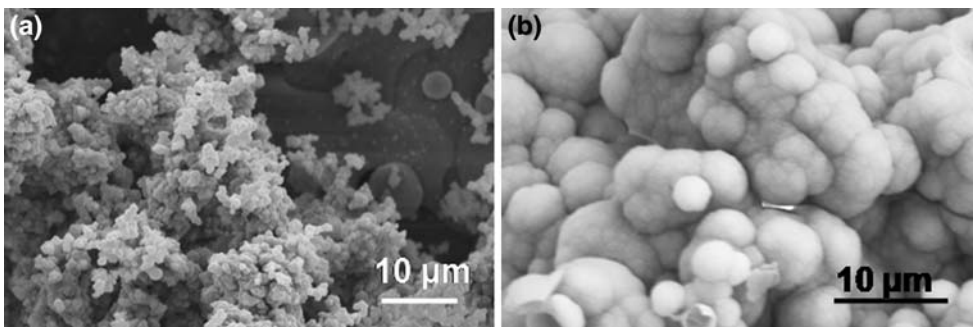

Fig. 1 Scanning electron micrographs of secondary hydroxyapatite coatings (top side coating) after incubation for (**a**) 28 and (**b**) 56 days in rSBF

carboxylate ligands such as citrate and oxalate delay the onset of HAp nucleation. However, not only the kinetics but also the morphology of precipitated HAp nanocrystals will be modified by structure-mediated (epitaxial) adsorption of organic constituents such as poly(amino acids) at prominent lattice planes of HAp [32]. Hence it is conceivable that the organic buffer [2-(4-(2-hydroxyethyl)-1-piperazinyl)ethan] sulfonic acid (HEPES) added to the simulated body fluid (rSBF) to suppress precipitation of calcium carbonate may play a role as an agent to delay the onset of nucleation of hydroxyapatite by a process akin to sterical hindering by the large bulky molecule similar to that suggested by Onuma et al. [33] for nucleation of calcium phosphate on a 11-mercaptoundecanoic acid self-assembled monolayer (SAM).

It is well known that such inhibitory effects in biological environments can usually be overcome by increasing the supersaturation of the solution [34, 35]. Hence in the present experiments an induction time was required to build up a high enough concentration level of Ca^{2+} and HPO_4^{2-} ions to substantially increase the supersaturation and to induce precipitation. This process is being mediated by dissolution of phases with higher solubilities, in particular amorphous calcium phosphate (ACP).The observed time lag is well in accord with earlier findings by Goetze et al. [36], Carayon and Lacout [37], Heimann et al. [38] and Tran [39]. Consequently, during longer incubation beyond 7 days a significant increase in the volume of the precipitate occurred as well as formation of larger structures (Fig. 1a). After 56 days, the surface of the as-sprayed coating was completely covered by a newly formed layer consisting of small spherical 'cauliflower-like' structures (Fig. 1b). This is in accord with findings by Jallot et al. [13] who also suggested that the largest precipitates grow and the smallest dissolve as a consequence of higher surface energy of smaller particles.

3.2 XRD phase analysis

Since the build-up of the coating by plasma spraying involves a rapid solidification process a significant percentage of metastable i.e. glassy phases will be formed that will commonly revert to more ordered, i.e. crystalline structures, during annealing at elevated temperatures or recrystallisation in contact with a solvent. On the other hand, it is expected that during precipitation of calcium phosphate from the simulated body fluid under physiological conditions predominately short-range ordered, i.e. more or less amorphous structures will be formed [40]. The results of phase determination using a Rietveld refinement routine are shown in Table 3 as a function of incubation time. It should be noted that by this technique only the crystalline components can be determined. Consequently ACP formed by rapid quenching of the molten droplets during plasma spraying and subsequently removed partially by dissolution in rSBF is excluded from Table 3.

Comparison with the chemical composition of the original spray powder revealed that the plasma spraying process changed considerably the phase composition of the initial HAp powder similar to work reported previously [1, 37, 38, 41]. Likewise, samples incubated for 28 days and beyond had lost their CaO content completely and $CaCO_3$ was formed instead, either by reaction with carbon dioxide from the surrounding air or, more likely by precipitation from the HCO_3^- containing rSBF. The high reactivity of CaO, its existence in the coating after incubation beyond 7 days, and the assumption that the X-ray penetration depth is less than 30 μm showed that the SBF initially influenced only the surfaces of the coatings and then gradually affected deeper regions by a rather slow inward diffusion process of water molecules [39, 42].

The crystalline content of as-sprayed coatings consisted of 72% HAp and approximately 28% of thermal decomposition products such as TTCP, TCP and CaO (Table 3). There is an understanding that an ACP phase is also present [41]. While its quantitative contribution was not determined in this study coatings using identical HAp powder and sprayed under virtually identical plasma conditions showed around 30 mass% of ACP in the as-sprayed coatings [39, 42]. Samples incubated for a period up to 28 days showed only small changes in their phase content, while the amount

Table 3 Crystalline phase content of the plasma sprayed HAp coatings in mass% [5, 14]

	HAp	TTCP	TCP	CaO	$CaCO_3$
Phase (mass%)					
Powder	97.6 ± 0.8	2.1 ± 0.55	0.3 ± 0.55	–	–
As-sprayed	71.8 ± 1.7	23.6 ± 1.6	3.3 ± 1.1	1.3 ± 0.3	–
Incubation time					
1 day	72.5 ± 1.5	23.5 ± 1.4	3.2 ± 1.0	0.7 ± 0.2	–
7 days	70.9 ± 2.3	21.8 ± 2.1	4.5 ± 1.3	0.4 ± 0.3	2.5 ± 0.8
28 days	70.6 ± 1.9	22.0 ± 2.0	6.2 ± 1.4	–	1.2 ± 0.9
56 days	82.8 ± 2.3	9.1 ± 1.9	6.2 ± 1.6	–	1.9 ± 0.7

of HAp phase present changed significantly after longer periods of incubation, increasing from approximately 71% after 28 days of incubation to approximately 83% after 56 days. In contrast to this, the amount of TTCP phase decreased strongly from 22% to 9%. This finding can be explained by the slow hydration kinetics of TTCP and the associated nucleation of HAp according to

$$3Ca_4O(PO_4)_2 + 3H_2O \leftrightarrow Ca_{10}(PO_4)_6(OH)_2 + 2Ca^{2+} + 4OH^- \quad (1)$$

Reaction (1) provides Ca^{2+} ions that continuously change the composition of the near-surface layer of the 'bone-like' Ca-deficient defect apatite coating with the general composition $(Ca_{10-z}(HPO_4)_z(PO_4)_{6-z}(OH)_{2-z} \cdot nH_2O,\ 0 \le z \le 1)$ towards precipitation of a highly porous but well-adhering stoichiometric HAp [43, 44].

The amount of tricalcium phosphate, TCP showed little changes. This is in contrast to the findings by Fazan and Marquis [45] who identified TCP as the calcium phosphate phase that forms hydroxyapatite in plasma-sprayed coatings by hydration according to [40, 41]

$$4Ca_3(PO_4)_2 + H_2O \leftrightarrow Ca_{10}(PO_4)_6(OH)_2 + 2Ca^{2+} + 2HPO_4^{2-} \quad (2)$$

An explanation for this discrepancy may be found in the fact that in the present experiments the plasma power (30–32 kW) was essentially higher than that applied in Ref. [45] (25 kW). In addition, using hydrogen as a secondary plasma gas instead of nitrogen used in Refs. [46, 47] increased the temperature of the plasma jet considerably so that formation of CaO occurred. Hence in the as-sprayed somewhat overheated coatings TCP was largely transformed to TTCP and CaO, respectively by evaporation of P_2O_5 according to

$$4Ca_3(PO_4)_2 \rightarrow 3Ca_4O(PO_4)_2 + P_2O_5 \uparrow \quad (3)$$

and

$$Ca_3(PO_4)_2 \rightarrow 3CaO + P_2O_5 \uparrow \quad (4)$$

The presence of substantial amounts of decomposition phases of hydroxyapatite such as TTCP and TPC in the incubated coatings even after 56 days testify to the sluggish dissolution/precipitation kinetics in the strongly buffered rSBF that follows the order of solubilities established by Ducheyne et al. [48]. The composition of the initially precipitated Ca-deficient defect apatite $Ca_{10-z}(HPO_4)_z(PO_4)_{6-z}(OH)_{2-z} \cdot nH_2O$ $(0 \le z \le 1)$ varies between that of amorphous calcium phosphate (ACP) $(z = 1)$ and hydroxyapatite $(z = 0)$. In neutral and slightly alkaline solutions the first product to appear is amorphous calcium phosphate (ACP) that serves as a template for heterogeneous nucleation of OCP that in turn leads to epitaxial growth of HAp [47]. In contrast, at higher pH of 10–11 the first phase to precipitate from an aqueous solution is OCP with $z = 2$ $(Ca_8H_2(PO_4)_6 \cdot 5H_2O$, OCP) that transforms very quickly to ACP, and then more slowly to Ca-deficient defect apatite that in turn gradually changes to HAp by uptake of Ca^{2+} and HPO_4^{2-} ions [40, 49–51]. This transformation has been described by a second-order kinetic law as a surface-reaction controlled process with surprisingly large activation energy of 95 kJ/mol [49]. It should be mentioned in passing that this high activation energy barrier will considerably be lowered in the presence of bone growth-mediating proteins such as osteocalcin that shows a high affinity for apatite and may play a role in cell signalling for bone formation [52]. Also, metabolic products such as citric acid and its salts appear to assist in bone-like bioapatite nucleation through their carboxylate terminal groups [31, 53]. Ab initio calculations provided evidence that Posner's cluster $[Ca_3(PO_4)_2]_3$ [54] is the energetically most stable configuration and that hydroxyapatite crystals may grow via such hexagonally close-packed left- and right-handed chiral clusters of 0.8 nm size [33, 55].

3.3 PIXE mapping

To study the temporal evolution of the composition of secondary HAp precipitated onto the coating surface during incubation in rSBF elemental maps of Ca, P and trace elements were obtained by irradiating the HAp coatings with protons. Figure 2 shows typical Ca maps of HAp coatings for incubation periods of 28 and 56 days, respectively obtained by irradiation with 1.5 MeV protons at a current of 300 pA. The elemental mapping was performed in the same locations where the SEM images (Fig. 1a, b) were taken. Table 4 shows the concentrations of elements together with their analytical uncertainties.

The distribution of Ca, P and trace elements was highly inhomogeneous over the probed area. However, the overall concentration levels for each incubation period could be clearly identified on these fully quantitative elemental maps. Not only the levels of concentration could be identified for every pixel but also a general overall measure of the concentrations could be inferred from the maps. From the elemental maps in Fig. 2, it can be observed that the average Ca concentration increased with increasing incubation time from 18 ± 5%, after 28 days to 30 ± 10%, after 56 days. The total content as obtained from the X-ray spectrum over the 250 μm^2 area (see Table 4) shows 19.1 ± 0.2% and 29.5 ± 0.3%, respectively. This signals an evolutionary trend towards fully stoichiometric HAp with a theoretical composition of 39.8% Ca. Similarly, the concentration of P increased with incubation time from

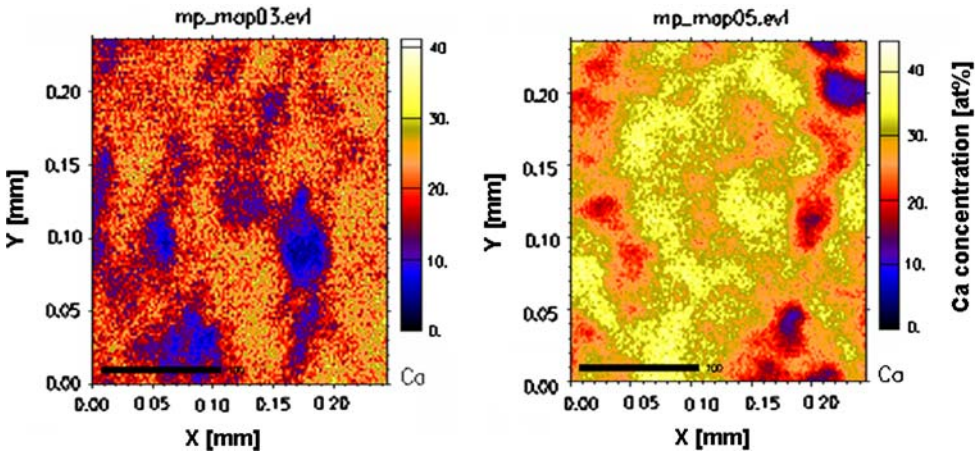

Fig. 2 Elemental maps of Ca obtained with 1.5 MeV protons, over micro-regions (approx. 250 × 250 μm^2) of selected areas of HAp coatings incubated for 28 (left) and 56 days (right). The beam probe diameter was approximately ~5 μm. Beam current intensity was ~200 to 400 pA; total accumulated charge was 0.162 and 0.504 μC, respectively

Table 4 Concentration levels of elements of HAp coatings incubated in rSBF as detected by PIXE

Species	Incubation time	
	28 days	56 days
Ca (%)	19.1 ± 0.2	29.5 ± 0.3
P (%)	6.6 ± 0.07	10.5 ± 0.1
Mg (%)	0.23 ± 0.04	0.48 ± 0.04
Ti (%)	n.d.	0.78 ± 0.013
S (μg/g)	184 ± 27	207 ± 27
K (μg/g)	n.d.	1,400 ± 127
Fe (μg/g)	89 ± 21	465 ± 31
Co (μg/g)	92 ± 19	113 ± 19
Sr (μg/g)	339 ± 92	346 ± 57

n.d.—Not determined

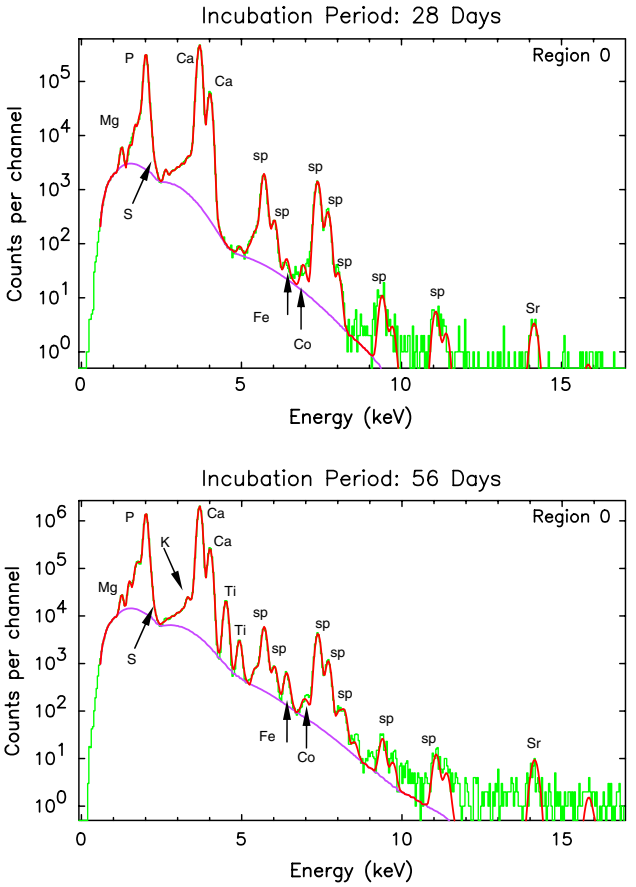

Fig. 3 Comparison of PIXE spectra of HAp coatings incubated for 28 (top) and 56 (bottom) days in rSBF. Major elements are Ca and P while an essential minor metabolic element is Mg. Sum peaks (sp) are due to high count rate of P and Ca X-ray lines arriving simultaneously at the Si(Li) detector

6.59 ± 0.07% after 28 days to 10.5 ± 0.1% after 56 days, and will presumably reach the value of 18.5% of stoichiometric HAp after much longer time.

Figure 3 shows the comparison of PIXE spectra obtained by irradiation of HAp coatings using beam energy of 1.5 MeV. Although only Ca and P are the elements of interest, the presence of minor elements such as Mg, S, K, Fe, Sr was noted and their positions are indicated in the figure. The elemental maps of hydroxyapatite powder show that the Sr originated from the spraying powder used in this study. The presence of these impurity ions may affect the precipitation kinetics as suggested above. It also appears that with increasing incubation time the precipitated Ca-deficient defect apatite incorporates Mg^{2+} and K^+ (Table 4) as well as CO_3^{2-} ions thus shifting its composition towards that of biological apatite. Presumably Na^+ ions will also be incorporated into the structure of HAp. However, for the applied experimental conditions it was not possible to detect Na with sufficient accuracy.

In addition, considerable amounts of Ti were detected in coatings incubated for 56 days. A tentative explanations can be based on a change in coating morphology during prolonged incubation in rSBF [44], in particular the occurrence of cracks propagating along the surface of the coating [5] that would enable the proton beam to penetrate to the substrate level. However, the titanium alloy may also

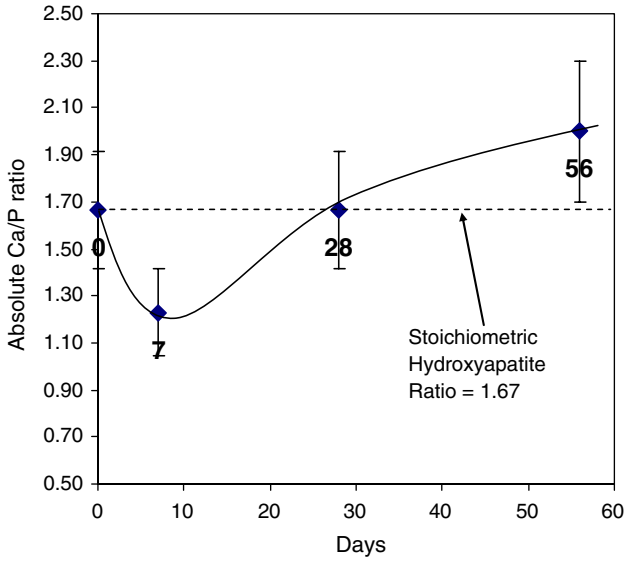

Fig. 4 Ca/P ratios of hydroxyapatite coatings incubated for 7, 28 and 56 days in rSBF obtained by RBS with 2 MeV alpha particles

release ions to the solution, as pointed out by Mu et al. [55] and linked to localised micro-detachments, indicating a very low capability of titanium to diffuse at a distance.

3.4 Rutherford backscattering spectrometry

Results of Rutherford backscattering spectrometry revealed a Ca/P ratio of approximately 1.25 after a short incubation time of 7 days as shown in Fig. 4. It was found previously that the first precipitate detectable after an incubation time of 7 days is a highly Ca-deficient defect apatite with a Ca/P ratio around 1.0 or below [38]. Longer contact with the simulated body fluid prompts the secondary hydroxyapatite to take up more of the Ca^{2+} ions released from the original as-sprayed coating by conversion of plasma-spray generated TTCP according to Eqs. 1 and 2, respectively [38, 44]. Consequently the Ca/P ratio of the secondary defect HAp increases towards that of stoichiometric HAp of 1.67. The PIXE data confirm this trend rather well. However, as evident from Fig. 4 the Ca/P ratio keeps increasing beyond an incubation time of 28 days to reach a value around 2.0 at 56 days. This ratio corresponds to tetracalcium phosphate, $Ca_4O(PO_4)_2$. Since it is difficult to reconcile this result with current wisdom additional work will be required to arrive at a reasonable explanation.

4 Conclusion

The changes of morphology and phase composition of plasma-sprayed hydroxyapatite coatings during in vitro incubation in rSBF were determined by quantitative analysis and elemental mapping using SEM, XRD, PIXE and RBS techniques.

The complementary information obtained by these analytical methods confirmed the formation of secondary hydroxyapatite by biomimetic processes, i.e. a dissolution–precipitation mechanism thought to be governing the mechanisms of osseoconductive integration of coated implants into living bone tissue. The application of PIXE provides a new tool to study bioconductive coatings and their in vitro alteration products, and therefore may contribute to the understanding of the nature of chemical bonding between bone and the HAp layer applied to metallic implant surfaces.

An induction time was required to build up a high enough concentration level of Ca^{2+} and HPO_4^{2-} ions to substantially increase the supersaturation and to induce precipitation even though the simulated body fluid used is highly supersaturated with respect to hydroxyapatite and OCP. In particular, SEM showed that a highly porous apatite layer formed at the surface of the coating after incubation for up to 28 days. Its morphology changed on further incubation for 56 days to a layer of 'cauliflower-like' spherulites composed of very fine crystallites, suggesting a high nucleation rate of calcium phosphate.

XRD phase analyses obtained by Rietveld refinement showed that the amount of HAp increased during incubation from 72 mass% in as-sprayed HAp coatings to 83% mass% after 56 days of incubation in rSBF suggesting both precipitation of secondary non-stoichiometric 'bone-like' hydroxyapatite from rSBF onto the coating surface and rehydration/recrystallisation of TTCP towards formation of HAp.

Spatially resolved PIXE elemental maps as well as RBS further confirmed that the concentration levels of Ca and P in the precipitated HAp layer increased with increasing incubation time confirming the notion of a gradual uptake of Ca^{2+} ions from the rSBF into the lattice of the Ca-deficient defect HAp thus changing its composition towards that of fully stoichiometric HAp.

Acknowledgements The authors are indebted to Ms. Margitta Hengst and Dr. Reinhard Kleeberg, both at the Department of Mineralogy, Technische Universität Bergakademie Freiberg for providing the hydroxyapatite coatings and the Rietveld refinement analyses, respectively. The authors are also grateful to Associate Professor Margit Härting, Department of Physics, University of Cape Town for discussions. The project was jointly sponsored by the German Federal Ministry of Education and Research (BMBF) and the National Research Foundation of the Republic of South Africa (NRF), Project Code 39.6.G0B.6.A.

References

1. K. DeGroot, R.T.G. Geesink, C.P.A.T. Klein, P. Serekian, Plasma-sprayed coatings of hydroxyapatite. J. Biomed. Mater. Res. **21**, 1375–1381 (1987)

2. R.B. Heimann, *Plasma-Spray Coating. Principles and Application* (Weinheim, Wiley-VCH, 2008)
3. Y.C. Tsui, C. Doyle, T.W. Clyne, Biomaterials **19**, 2015–2029 (1998)
4. Y.C. Tsui, C. Doyle, T.W. Clyne, Biomaterials **19**, 2031–2043 (1998)
5. M. Topić, T. Ntsoane, R.B. Heimann, Surf. Coat. Technol. **201**(6), 3633–3641 (2006)
6. D.F. Williams (ed.), *Concise Encyclopedia of Medical and Dental Materials. Advances in Materials Science and Technology* (Pergamon Press, Oxford, 1990)
7. G. Heimke (ed.), *Osseo-integrated Implants* (CRC Press, Boca Raton, 1991)
8. L.L. Hench, J. Am. Ceram. Soc. **74**(7), 1487–1510 (1991)
9. R.Z. LeGeros, J.P. LeGeros, in *Phosphate Minerals*, ed. by J.O. Nriagu, P.B. Moore (Springer, New York, 1984), pp. 351–385
10. R.B. Heimann, Mat-wiss u Werkstofftechn. **30**, 775–782 (1999)
11. H.M. Kim, T. Miyazaki, T. Kokubo, T. Nakamura, Bioceramics **13**, 47–50 (2001)
12. R.B. Heimann, in *Engineering Mineralogy of Ceramic Materials*, ed. by M. Mellini, B. Messiga (University Press, Siena, 2002), pp. 117–134
13. E. Jallot, H. Benhayoune, G. Weber, G. Balossier, P. Bonhomme, J. Phys. D: Appl. Phys. **33**, 321–326 (2000)
14. T. Huettel, Mechanical and microstructural characterisation of plasma-sprayed bioconductive hydroxyapatite coatings on Ti6Al4V. Unpublished Master Thesis, Technische Universitat Bergakademie Freiberg, Freiberg, Germany, 2003
15. V.M. Prozesky, W.J. Przybylowicz, E. van Achterbergh, C.L. Churms, C.A. Pineda, K. Springhorn, J.V. Pilcher, C.G. Ryan, J.H. Kritzinger, T. Schmitt, Nucl. Instr. Meth. B. **104**, 36–42 (1995)
16. W.J. Przybylowicz, J. Mesjasz-Przybylowicz, C.A. Pineda, C.L. Churms, C.G. Ryan, V.M. Prozesky, R. Frei, J.P. Slabbert, J. Padayachee, W.U. Reimold, X-ray Spectrometry **30**, 156–163 (2001)
17. W.J. Przybylowicz, J. Mesjacz-Przybylowicz, C.A. Pineda, C.L. Churms, V.M. Prozesky, X-ray Spectrometry **28**, 237–243 (1999)
18. C.G. Ryan, E. van Achterbergh, C.J. Yeats, T.T. Win, G. Cripps, Nucl. Instr. Meth. B. **189**, 400–407 (2002)
19. L.R. Doolittle, Nucl. Instr. Meth. B. **9**, 344–351 (1985)
20. J.F. DeRooi, J.C. Heughbaert, G.H. Nancollas, J Colloid Interface. Sci. **194**(100), 350–358
21. T.P. Feenstra, P.L. DeBruyn, J. Phys. Chem. **83**, 465–479 (1979)
22. J.L. Heughebaert, S.J. Zawacki, G.H. Nancollas, J. Cryst. Growth **63**, 83–90 (1983)
23. P. Koutsoukos, Z. Amjad, M.B. Tomson, G.H. Nancollas, J. Am. Chem. Soc. **102**, 1553–1557 (1980)
24. X. Lu, Y. Leng, Biomaterials **26**(10), 1097–1108 (2005)
25. M.H. Salimi, J.C. Heughebaert, G.H. Nancollas, Langmuir **1**, 119–122 (1985)
26. E.D. Eanes, S.L. Ratner, J. Dental Res. **60**, 1719–1723 (1981)
27. E. Landi, A. Tampieri, G. Celotti, S. Sprio, M. Sandri, G. Logroscino, Acta Biomater. **3**(6), 961–969 (2007)
28. H.J. Meyer, The influence of impurities on the growth rate of calcite. J. Cryst. Growth **66**(3), 639–646 (1984)
29. R. Rosmaninho, L.F. Melo, The effect of citrate on calcium phosphate deposition from simulated milk ultrafiltrate (SMUF) solution. J. Food Eng. **73**(4), 379–387 (2006)
30. C.E. Fowler, M. Li, S. Mann, H.C. Margolis, Influence of surfactant assembly on the formation of calcium phosphate materials—A model for dental enamel formation. J. Mater. Chem. **15**, 3317–3325 (2005)
31. P.F. Schofield, E. Valsami-Jones, I.R. Sneddon, J. Wilson, C.A. Kirk, N.J. Terrill, C.M. Martin, D. Lammie, T.J. Wess, Nucleation and growth of nano-apatite: applications to biomineralisation. Geochim. Cosmochim. Acta **69**(10), A 72 (2005)
32. S.I. Stupp, P.V. Braun, Molecular manipulation of microstructures: biomaterials, ceramics, and semiconductors. Science **277**, 1242–1248 (1997)
33. K. Onuma, A. Oyane, T. Kokubo, G. Treboux, N. Kanzaki, A. Ito, Precipitation kinetics of hydroxyapatite revealed by the continuous-angle laser light-scattering technique. J. Phys. Chem. B. **104**, 11950–11956 (2000)
34. S. Mann, Mineralization in biological systems. Struct. Bond. **54**, 125–174 (1983)
35. S. Mann, Molecular recognition in biomineralization. Nature **332**, 119–124 (1983)
36. J. Goetze, H. Hildebrandt, R.B. Heimann, Charakterisierung des in vitro-Resorptionsverhaltens von plasmagespritzten Hydroxylapatit-Schichten. BIOmaterialien **2**, 54–60 (2001)
37. M.T. Carayon, J.L. Lacout, Study of the Ca/P atomic ratio of the amorphous phase in plasma-sprayed hydroxyapatite coatings. J. Solid State Chem. **172**, 339–350 (2003)
38. R.B. Heimann, O. Grassmann, T. Zumbrink, H.P. Jennissen, Biomimetic processes during in vitro leaching of plasma-sprayed hydroxyapatite coatings for endoprosthetic applications. Mat-wiss u Werkstofftech. **32**, 913–921 (2001)
39. H.V. Tran, Investigation into the thermal dehydroxylation and decomposition of hydroxyapatite during atmospheric plasma spraying: NMR and Raman spectroscopic studies of as-sprayed coatings and coatings incubated in simulated body fluid. Unpublished PhD Thesis, Technische Universitat Bergakademie Freiberg, Freiberg, Germany, 2004
40. R.B. Heimann, in *Trends in Biomaterials Research*, ed. by P.J. Pannone (Nove Science Publishers Inc., Hauppauge, NY, 2007), pp. 1–81
41. K.A. Gross, V. Gross, C.C. Berndt, J. Am. Ceram. Soc. **81**(1), 106–112 (1998)
42. R.B. Heimann, R. Wirth, Biomaterials **27**, 823–831 (2006)
43. R.B. Heimann, H.V. Tran, P. Hartmann, Mat-wiss u Werkstofftech. **34**(12), 1163–1169 (2003)
44. O. Grassmann, R.B. Heimann, J. Biomed. Mater. Res. **53**(6), 685–693 (2000)
45. F. Fazan, R.M. Marquis, J. Mater. Sci.: Mater. Med. **11**, 787–792 (2000)
46. K. DeGroot, Biomaterials **1**, 47–52 (1980)
47. H. Monma, S. Ueno, T. Kanazawa, J. Chem. Tech. Biotechnol. **31**, 15–24 (1981)
48. P. Ducheyne, S. Radin, L. King, J. Biomed. Mater. Res. **27**, 25–34 (1993)
49. C. Liu, Y. Huang, W. Shen, J. Cui, Biomaterials **22**, 301–306 (2001)
50. R.Z. LeGeros, G. Daculsi, I. Orly, T. Abergas, W. Torres, Scan Microsc. **3**, 129–138 (1989)
51. R.B. Heimann, J. Thermal Spray Technol. **8**(4), 597–604 (1999)
52. Q.Q. Hoang, F. Sickeri, A.J. Howard, D.S.C. Yang, Nature **425**, 977–980 (2003)
53. P.G. Robey, Connect. Tissue Res. **35**, 185–190 (1996)
54. A.S. Posner, F. Betts, Acc. Chem. Res. **8**, 273–281 (1975)
55. Y. Mu, T. Kobayashi, M. Sumita, A. Yamamoto, T. Hanawa, J. Biomed. Mater. Res. **49**, 238–243 (2000)